

Triboelectric performances of self-powered, ultra- flexible and large-area poly(dimethylsiloxane)/Ag-coated chinlon composites with a sandpaper-assisted surface microstructure

Lixiao Li¹, Su Liu², Xiaoming Tao², and Jian Song^{1,*}

¹ *Guangdong Provincial Key Laboratory of Durability for Marine Civil Engineering, Shenzhen University, Shenzhen 518060, China*

² *Nanotechnology Center of Functional and Intelligent Textiles and Apparel, Institute of Textiles and Clothing, The Hong Kong Polytechnic University, Kowloon, Hong Kong, China*

Abstract

Apart from the rapid development in macroscale green energies, such as wind energy and hydro energy, micro/nanoscale self-powered energy systems are increasingly attractive in wearable energy systems. To utilize the energy harvester more conveniently and effectively, an energy harvester, viz., single-electrode textile-based triboelectric nanogenerator (ST-TENG), is reported in this study. The ST-TENG is a polydimethylsiloxane (PDMS)/Ag-coated chinlon fabric (PACF) composite film with the surface microstructures induced by sandpapers. The PACF composite is self-powered based on the triboelectrification and electrostatic induction. The merits of ST-TENG include: (1) all the basic materials are flexible and scalable; (2) the resultant PACF is a free-standing composite film, which can be easily peeled off from the sandpaper substrate; (3) an extremely low-cost method was first introduced to fabricate the surface microstructures in flexible triboelectric nanogenerator though sandpapers; and (4) the as-fabricated PACF composite film can directly harvest energy though squeezing, warping and folding. Experimental results demonstrate that the ST-TENG can generate an average maximum output voltage of 46.52 V and a high-power density of 613 mWm⁻² at the external resistance of 20 MΩ. Additionally, the ST-TENG can also be utilized to detect the variation of contact area, frequency and force.

Introduction

Textile-based photonic and electronic systems, which are permeable and light, can be made in very large areas over hundreds or thousands of square meters [1–4]. However, providing flexible, green, large-scale, easily fabricated and convenient-to-utilize power sources for the aforementioned systems remains a challenging and arduous task [5]. As a consequence, flexible textile-based triboelectric nanogenerators (T-TENG) were proposed and have drawn huge attention to micro/nano-energy fields, as they can harvest energy from common human motions by a conjunction of triboelectrification and electrostatic induction [6]. Water-driven [7, 8], wind-driven [9, 10] and motion-driven [11, 12] TENGs have experienced a rapid development in recent years, and most of the TENGs have two electrodes to provide a closed circuit for the flow of electrons induced by electrostatic induction. Although this configuration is available to harvest mechanical energy, it is difficult for practical applications, i.e., harvesting energy from a rotating motion or fixing the electrodes in motion body. Therefore, another kind of nanogenerator, viz., single-electrode nanogenerator (S-TENG), has been proposed, i.e., fingertip-driven TENG [13, 14]. This new type of nanogenerator is found to be more practical and feasible for real-life applications, since S-TENG with single electrode can harvest

energy by conveniently contacting others.

Guo et al. [14] reported a graphene oxide-based S-TENG, which can not only harvest mechanical energy, but also enable detecting the dynamic force triggered by hand touch. Yang et al. [15] presented a S-TENG to harvest diverse forms of mechanical energy. It is quite convenient for harvesting energy through pressing the arch-shaped polytetrafluoroethylene (PTFE) film to fulfill the contact-separation motion. Shi et al. [16] fabricated a single-electrode textile-based nanogenerator (ST-TENG) through a facile dip-coating method; however, such a method could not maintain the virgin shape of conductive fabric in the dip-coating process. Nevertheless, the ST-TENGs were known to have relatively low output electric performances compared to the TENGs with two electrodes, because only the tribo-charges on the surface of the dielectric material connecting with the electrode have a contribution to inducing the electronic transformation between the electrode and ground. Hence, apart from choosing basic materials with larger polarization difference, creating surface micro/nanostructures is another excellent approach to further enhance the electric performances of TENGs. Nowadays, surface etching and surface replication are two primary approaches to form micro/nanostructures [17–21]. For the former, Lin et al. [20] fabricated the polymer nanowire structures on the contact surfaces via inductively coupled plasma (ICP) etching. Lee et al. [22] used a reactive ion etching (RIE) nanotechnology to develop the nanostructured configuration of contact material surface; a 4.6 times higher current enhancement was achieved based on the nanopatterned T-TENG compared to the T-TENG with a flat surface. For the latter, currently, many surface microstructures, such as pyramids [23, 24], cube [25] and nanorod array [26], have been investigated by copying the surface configurations of the mold. However, additional post-processes, i.e., transferring/integrating the as-fabricated dielectric to the electrode, are essential for fabricating the TENG, giving rise to a multi-step technology [27]. Likewise, the cost of the manufacture mold and surface micro/nano-manufacture also increase the manufacturing costs and limit the size of TENG. Therefore, the development of facile, inexpensive and one-step manufacturing technology to generate surface microstructures on the contact surface in TENGs is considerably important.

In this work, an ultra-flexible and large-scale polydimethylsiloxane (PDMS)-based Ag-coated chinlon composite was fabricated by using a facile and one-step doctor-blending technology. The commercially knitted Ag-coated chinlon fabric (ACF) and PDMS polymer were adopted as the original materials. The PDMS has been widely used as a promising multifunctional soft matter as it has many advantages—high flexibility and biocompatibility [28, 29]. More significantly, inexpensive sandpapers were first used to generate surface microstructures on flexible TENG in the one-step process, without any complex or expensive post-treatment. Due to the rough surface, the resultant PACF can be easily peeled off from the sandpaper substrate and directly used as a single-electrode energy harvester, viz. ST-TENG. The corresponding operation principle has been elaborated by finite element simulation. The maximum power density of the ST-TENG with a microstructure induced by the sandpaper of P3000 (P^* is the roughness class of sandpaper) can reach up to 613 mWm^{-2} , which can light up 8 LEDs by squeezing motion and 20 LEDs by flapping motion. The method and findings from this study are expected to be helpful to design the textile-based nano-energy system in a more facile, practical and low-cost manner.

Materials and methods

Materials

The elastomer for the PDMS and the related cross-linking agent were purchased from Momentive Performance Materials, Japan LLC. The flexible and antibacterial ACF was obtained from LuFeierTM. Inexpensive sandpapers (Matador, German) with different surface roughnesses were used to form the convex–concave surface morphology.

Fabrication of PACF

PDMS and cross-linking agent were homogeneously mixed with a mass ratio of 1:1 to fabricate the PDMS mixed solution. A sandpaper substrate was attached to a glass panel using double-sided tapes, where the use of adhering tapes on each side of the sandpaper is to fix the position of substrate and, more importantly, to determine the thickness of the PDMS film.

Afterward, the resultant mixed solution was casted at one end of the sandpaper, and subsequently coated on the sandpaper surface via an extremely facile doctor-blading method assisted by a glass rod. Likewise, the ACF was uniformly covered on the surface of the PDMS film. After curing at 80 °C for 30 min in an oven, the PACF was fabricated and could be easily peeled off from the sandpaper substrate. Figure 1a shows the schematic illustration of the fabrication process. The practical process can be also found in Figure S1, ESI.

The as-fabricated PACF was cut into several small samples with surface area of 60×60 mm², and used to investigate the triboelectric properties. Additionally, to investigate the mechanical properties of PDMS film, a PDMS film with a size of 60 mm×10 mm×3.689 μm was fabricated using the same synthetic method, and two double-side tapes with a 10 9 20 mm² area were stuck to the end of the sample (Figure S2c, SI).

Material characterization

The morphology and element were measured by scanning electron microscopy (SEM, Tescan VEGA3) and FTIR spectrometry (Spectrum 100, PerkinElmer US). The surface roughness was obtained by a 3D optical surface profile (Zygo, Nexview).

Performance measurement

The mechanical properties of the PDMS were measured by a Material Test System (Instron5944, RT2kN), and the experimental setups and method can be found in Figure S2a, SI. The output performance of the nanogenerator was evaluated by utilizing a Keyboard Life Tester (ZXA03), which can provide a continuous dynamic sinusoidal motion with controlled displacement levels ranging from 0 to +10 mm and frequency levels ranging from 1 to 5 Hz. The force signal was monitored by a DAQ (Dewetron, Dewe-2600 DAQ system) system. Meanwhile, the voltage signal was collected by a Keysight DSO-X3014A oscilloscope and an N2790A high-voltage probe with 8 MX internal resistance (the corresponding setup can be seen in Figure S3, SI, and the corresponding internal circuit of Oscilloscope can be found in Figure S4, SI).

Results and discussion

Fabrication of the PACF film

The PACF was fabricated by an extremely facile doctor-blending

technology (Fig. 1a), and the detailed fabrication process can be found in “Materials and methods”. The as-fabricated PACF possesses many advantages, including: (1) extremely inexpensive sandpapers ($\sim \$0.0025 \text{ cm}^{-2}$) were used to fabricate the surface microstructures of the polymer; (2) the as-fabricated PACF was a free-standing composite film, which can be easily peeled off from the rough surface of the sandpaper substrate (Fig. 1b); (3) the flexible PDMS (modulus of 1.59 GPa) and the ultra-flexible, large-scale and biocompatible ACF (electric resistance: $\sim 0.1 \Omega$) were selected as the original materials (Fig. 1c); (4) the PACF can directly output charge based on the triboelectric effect though squeezing, warping and folding motions (Fig. 1d).

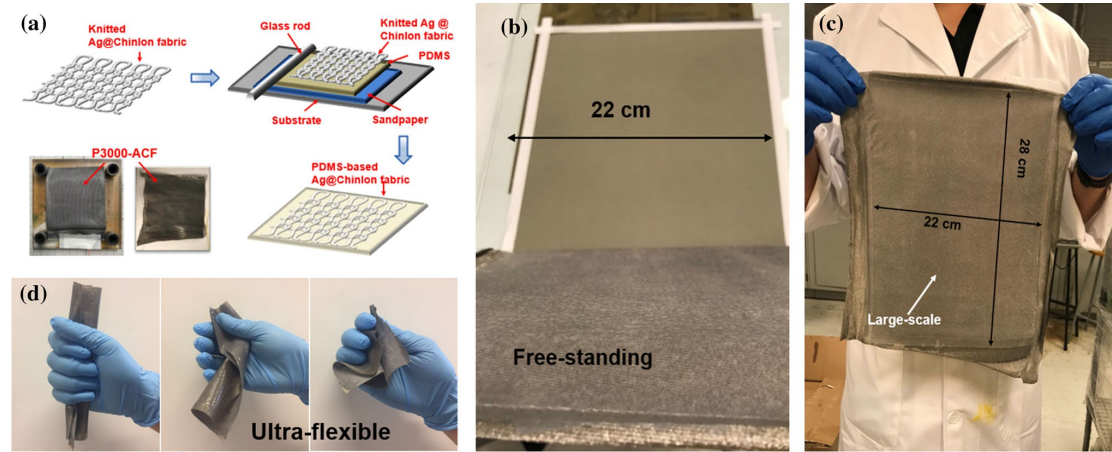


Figure 1 a Schematic images of one-step fabrication process for PACF with the surface microstructures and the practical image of as-fabricated PACF. b, c An ultra-flexible, large-scale and free-standing PACF composite film, which can be easily peeled off from the sandpaper substrate. d Photographs of an ultra-flexible PACF, which can be squeezed, warped and folded.

Structure and characterization of the PACF film

Figure 2a, b illustrates the cross-sectional area morphology of the as-fabricated PACF, where the one-side ACF is closely surrounded by the PDMS polymer. By mechanically triggering human motions, i.e., squeezing and folding motions, the tribo-charges can be easily transferred through the ACF electrode in the single-electrode TENG mode. Furthermore, the uniform distribution of the as-fabricated microstructures (microholes) on the surface of the PDMS film (Fig. 2c) demonstrates that the sandpaper can provide an effective, facile and extremely low-cost route to manufacture the specific surface micro/nanostructures. Figure 2d qualitatively exhibits the surface roughness class of the various microstructures. With the increases of sandpaper mesh, the surface of PDMS obviously becomes smoother and the roughness decreases from $10.899 \mu\text{m}$ to $2.635 \mu\text{m}$.

The FTIR spectrum shown in Fig. 2e confirms that the synthesized resultant is the PDMS polymer. It could be noted from the mechanical response of the PDMS film (Fig. 2f) that the modulus and yield strength of the PDMS film are 1.59 GPa and 0.4 MPa, respectively. It indicates that the polymer is flexible and can be incorporated into a wearable device.

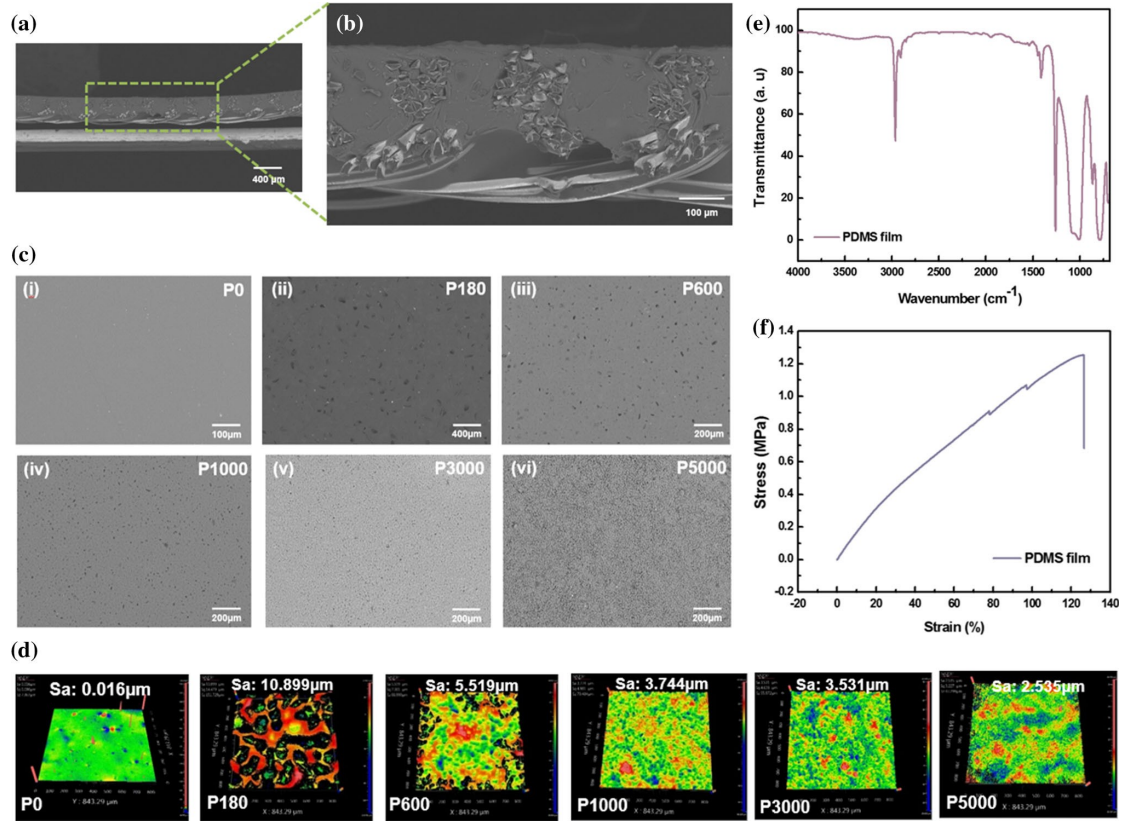


Figure 2 a, b SEM images of the PACF cross section. c SEM images of surface microstructures. d Surface roughness of PDMS film induced by different sandpapers. e FTIR spectrum of PDMS film. f Stress versus strain curve of PDMS film.

Triboelectric working mechanism of the PACF as an ST-TENG

To quantitatively investigate operation principle of the PACF as an ST-TENG, a finite element model (FEM) was built up to simulate the electric potential distribution using COMSOL[®], as shown in Fig. 3. Here, the FEM corresponds to the contact–separation mode between a skin patch and a PACF which is connected to the ground. The width and thickness of the PDMS film are 1.48 mm and 200 μm , respectively. The microstructures on the PDMS film induced by sandpaper are simulated by 16 rectangles (area $37 \mu\text{m} \times 3.7 \mu\text{m}$). The tribo-charges on the skin and PDMS film are assumed to be $\pm 1 \mu\text{C}$. Figure 3 exhibits the simulated results of the potential distribution in ST-TENG under different separation distances of 0, 0.1, 0.3, 0.5 and 0.6 mm. In the case of full contact between the skin and PDMS, there is no potential difference in ST-TENG. The potential difference dramatically rises with the increase of separation distance. In the case of 0.6 mm distance, the potential on the skin is up to $\sim 1.83\text{e}4 \text{ V}$, and a relatively small potential can be found within the PDMS film. As shown in Fig. 3c, the relationship between the potential on the skin and the distance exhibits obvious nonlinear trend, owing to the satisfaction phenomenon induced by tribo-charges between the skin and PDMS. Due to the single-electrode working mode, the ST-TENG is a more practical and facile design for some applications, i.e., skin-driven ST-TENG [15, 30]. Figure 3d illustrates the operation mechanism of the ST-TENG, where the rough surface of the PDMS was sketched by using several rectangular blocks. In accordance with the triboelectric series, PDMS and human skin can be considered as triboelectrically negative and positive materials due to their different

electronegativity. Initially, after sufficient contact, equal charges with opposite polarity induced by the triboelectric effect were uniformly distributed on the two contact surfaces, where the PDMS layer was negatively charged and the human skin was positively charged (Fig. 3d, i). When the skin was separated from the PDMS, an electrical potential difference was built and caused electronics flow from Ag electrode to the ground to balance the negative charges on the surface of the PDMS (Fig. 3d, ii). An electrostatic equilibrium was achieved when the skin and the PDMS reached the maximum separation distance (Fig. 3d, iii). As the skin moved back, the process was reversed and a charge flow along the opposite direction emerged (Fig. 3d, iv).

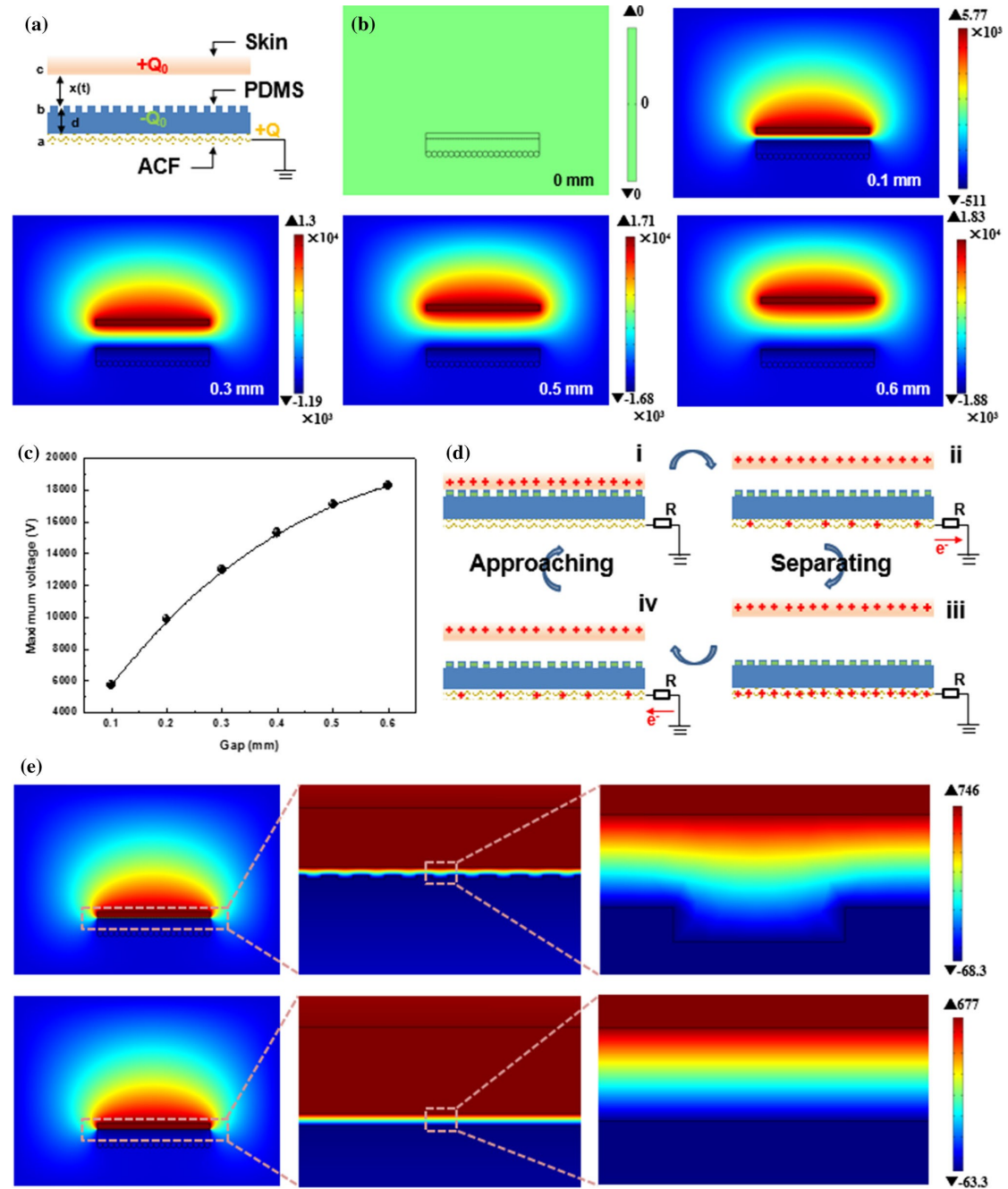


Figure 3 ST-TENG in contact-separation mode. a Schematic illustration of the model for calculation. b The potential distribution obtained by finite element simulation in ST-TENG for the variation of gap between the skin and PACF. c Maximum potential in ST-TENG as a function of the gap. d Sketches illustrating the working principle. e

Comparison of the potential distribution in ST-TENGs with/without the surface microstructures.

In addition, Fig. 3e shows the comparison results of the ST-TENG with/without the surface microstructures. The maximum voltage of the ST-TENG with the surface microstructure is obviously higher than that without the microstructure, improved by ~ 70 V, which can be ascribed to the increase of gap and local deformation in the contact surface. Hence, the extremely inexpensive sandpapers can be used as a master to create the microstructures on the surface of the PDMS film.

Triboelectric performances of the PACFs as an ST-TENG

Surface roughness has a remarkable effect on the electric performances of nanogenerators [31–33]. Figure 4a shows the output voltage–time curves of the ST-TENG based on the PACF film with different surface roughnesses induced by P0, P180, P600, P1000, P3000 and P5000 sandpapers, respectively. Among them, the P3000-ST-TENG shows the best output voltage compared to others, which can be attributed to the comprehensive effect of surface microstructures and contact surface size. In fact, the increase of the microstructure density can improve the effective contact surface owing to the larger local elastic deformation of the PDMS film in the contact–separation process. However, too many such microstructures [viz., microholes (Fig. 2c)] can severely reduce the effective contact area and result in the decrease of electric performance of the ST-TENG (Fig. 4a).

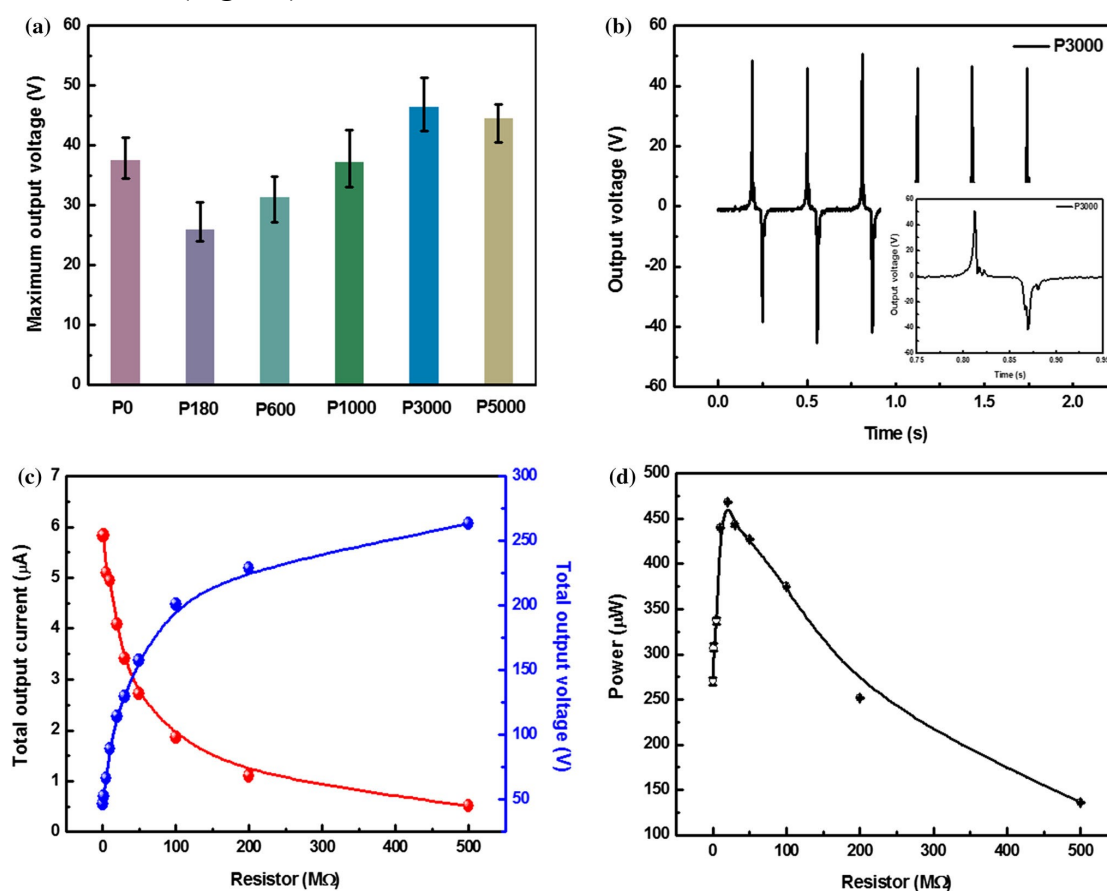


Figure 4 Triboelectric performances of ST-TENG. a Influence of roughness of sandpapers on the maximum output voltage of ST-TENG. b Typical output voltage versus time curve based on the P3000-ST-TENG. The inset image is the magnified image of voltage–time curve. c Influences of load resistors on the total output current

and voltage. d Power output as a function of load resistors.

Figure 4b illustrates the typical output voltage versus time based on a P3000-ST-TENG driven by a cyclic compression force of 500 N at a frequency of 3.24 Hz and contact area of 762.73 mm². The average maximum output voltage was 46.52 V. The existence of surface microstructures and ultra-flexible materials of the ST-TENG also make some local contact–separation phenomena, giving rise to some additional charges, as shown in Fig. 4b, inset image. Figure 4c, d demonstrates the resistance dependence via adopting an external resistor varying from 0.1 M Ω to 500 M Ω ; the corresponding electric circuit is shown in Figure S3, ESI. With the increase of resistance, the current amplitude declines and the measured voltage with respect to the internal resistor (8 M Ω) rises (Fig. 4c). The instantaneous power shows a maximum value of 613 mWm⁻² at the external resistance of 20 M Ω .

Influences factors on the triboelectric performances of the PACF as an ST-TEGN

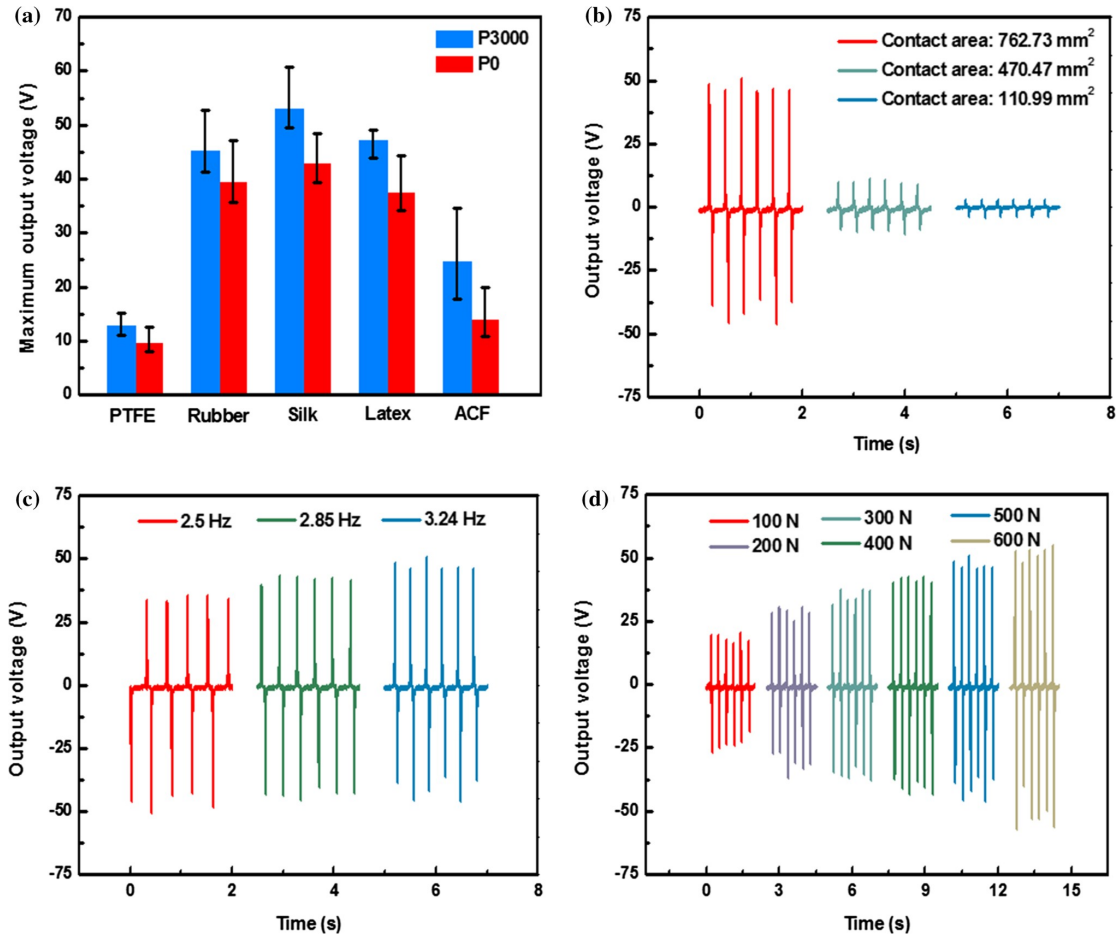


Figure 5 Influences of different triboelectric layers (a), contact areas (b), frequencies (c) and forces (d) on the triboelectric performances of the ST-TENG.

In practical application, many factors, such as tribo-materials, contact areas, frequencies and forces, play a great role in the electric responses of the ST-TENGs. Therefore, the above-mentioned impact factors are systematically investigated in this section. Figure 5a exhibits the maximum output voltages corresponding to various tribo-materials under the maximum force of 500 N at a frequency of 3.24 Hz. It is noted that the P3000-ST-TENG has a higher electric performance than P0-ST-TENG for all materials. Although the ST-TENG based on

the silk material can generate a relatively high output voltage in comparison to those based on rubber and latex, it is more convenient to wear a rubber-based or latex-based glove as the object to create the tribo-charges between the object and PDMS.

Figure 5b–d shows the influences of the contact areas, frequencies and force on the electric performances of P3000-ST-TENG. For Fig. 5b, the output voltage behavior was mechanically triggered by a dynamic impact force of 500 N at a frequency of 3.24 Hz, which significantly declined with the decrease in the contact area. In Fig. 5c, d, the maximum output voltage experiences a gradual rise process with the increases in the frequency or force, confirming a potential application of the as-fabricated single electrode as a sensor to monitor human motions.

Applications of the PACF as an ST-TENG

On the basis of the strong advantages of the ultra-flexible and large-scale ST-TENG demonstrated above, the P3000-PACF was used as a smart single-electrode energy harvester and load sensor by repeatedly contacting and separating with the hand (skin) (Fig. 6). The considered ST-TENG has a 6 cm × 6 cm surface area, and the microstructure on the surface was formed assisted by the P3000 sandpaper based on the aforementioned doctor-blading method. In Fig. 6a, eight LEDs were in series connected with the ST-TENG and ground. In accordance with the aforementioned operation mechanism, eight LEDs can be directly lighted by repeated squeezing (Fig. 6a–c, Movie S1, ESI). In Fig. 6b, 20 LEDs, the ST-TENG, and ground were connected in series by Cu wire, in which the patch board was used to fix the 20 LEDs. By flapping motion, the ST-TENG can drive 20 LEDs via a facile flapping motion (Fig. 6d, e, Movie S2, ESI). Therefore, the results confirm that the as-fabricated ST-TENG can be used as an energy harvester to scavenge mechanical energy.

Moreover, to test the stabilization of the overall circuit under squeezing, warping and folding motion, the conductivity of the PACF composites was experimentally studied and the corresponding results are shown in Figure S5, EI. The measured change in conductivity of the PDMS was marginal, indicating that the PACF is suitable to be used as a wearable device for application.

In addition to harvesting mechanical energy, an output signal of the ST-TENG corresponding to the contact–separation motion (named as squeezing motion) was obtained, which can be used as a load sensor to monitor the movement status. In Fig. 6f–h, the ST-TENG was connected with a Keisight DSO-X3014A oscilloscope to directly record the relationship between the output voltage behavior of the ST-TENG and the motion case, in which the terminal of the oscilloscope was connected with the ground. An output voltage signal was generated by the squeezing-releasing motion as shown in Fig. 6g (Movie S3, ESI). Specifically, one semi-cycle output voltage corresponded to one squeezing or releasing motion, and there was a positive correlation between the signal absolute intensity and pressure. Therefore, the output signal can reflect the variation of load and frequency.

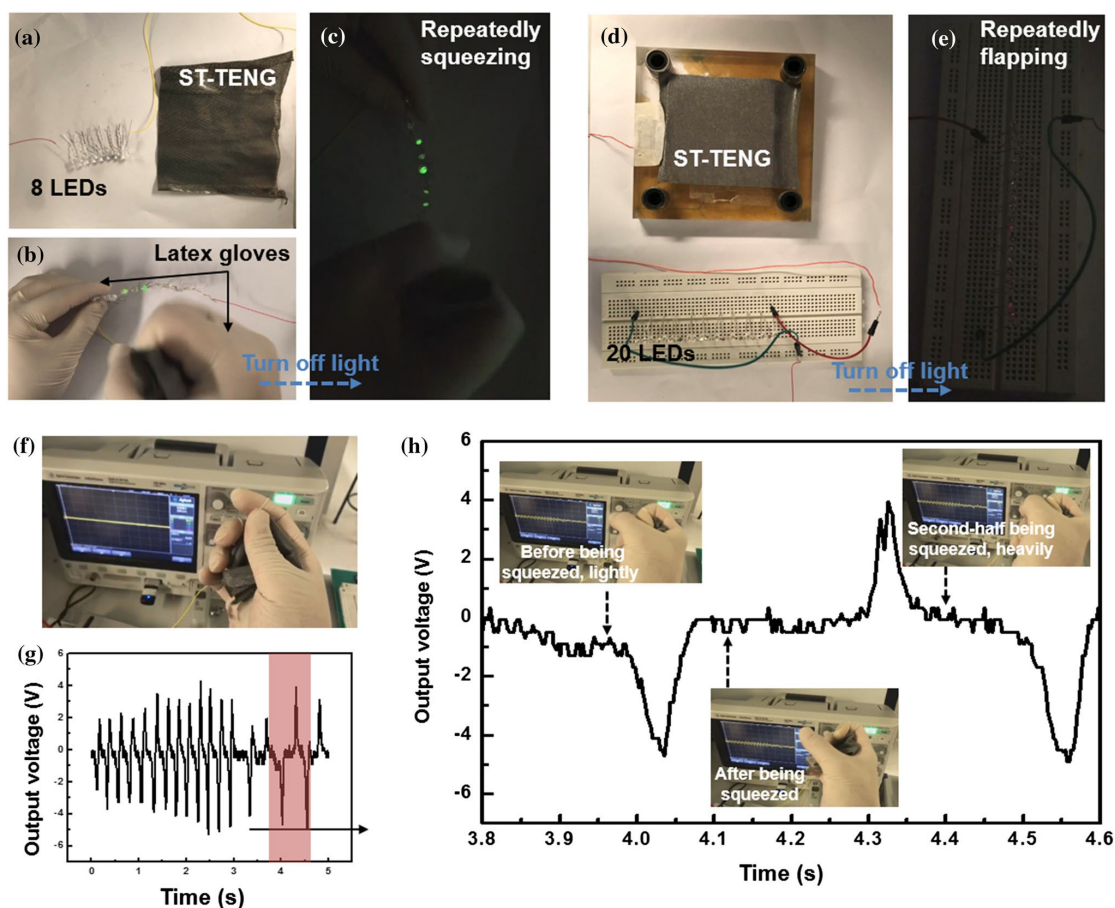


Figure 6 Applications of ST-TENGs a–c Lighting of eight LEDs by repeatedly squeezing the ST-TENG. d–e Lighting of 20 LEDs by repeatedly flapping the ST-TENG. f–h Load sensor based on ST-TENG, driven by repeatedly squeezing the ST-TENG.

Conclusions

Based on a facile doctor-blending technology, an ultra-flexible, large-scale and free-standing PACF with surface microstructures has been successfully fabricated, which can be directly used as a single-electrode textile-based nanogenerator. By using extremely low-cost sandpapers, the surface microstructures can be generated on the surface of the PDMS film. Additionally, due to the rough surface of the sandpaper, the as-fabricated PACF could be easily peeled off from the sandpaper substrate. A power density of 613 mWm^{-2} at the external resistance of $20 \text{ M}\Omega$ was obtained. The ST-TENG can drive 8 LEDs by squeezing the PACF and 20 LEDs by flapping the PACF. Because the electric performance is sensitive to the contact area, frequency and force, the ST-TENG can also be used as a sensor to monitor human motions.

Acknowledgements

The financial support for this research has been provided by the National Natural Science Foundation of China (Grant No. 51778373), the Knowledge Innovation Project of Shenzhen (Grant No. JCYJ20170302143625006) and New Teacher Program of Shenzhen University (Grant No. 2016066).

Electronic supplementary material: The online version of this article (<https://doi.org/10.1007/s10853-019-03428-5>) contains supplementary material, which is available to authorized users.

References

1. Tao X (2015) Handbook of smart textiles. Springer, Singapore
2. Song J, Yang B, Zeng W, Peng Z, Lin S, Li J, Tao X (2018) Highly flexible, large-area, and facile textile-based hybrid nanogenerator with cascaded piezoelectric and triboelectric units for mechanical energy harvesting. *Adv Mater Technol* 3:1800016–1800031. <https://doi.org/10.1002/admt.201800016>
3. Park S, Jayaraman S (2003) Smart textiles: wearable electronic systems. *MRS Bull* 28(8):585–591
4. Liu M, Pu X, Jiang C, Liu T, Huang X, Chen L, Du C, Sun J, Hu W, Wang ZL (2017) Large-area all-textile pressure sensors for monitoring human motion and physiological signals. *Adv Mater* 29(41):1703700–1703709
5. Wen Z, Yeh MH, Guo H, Wang J, Zi Y, Xu W, Deng J, Zhu L, Wang X, Hu C (2016) Self-powered textile for wearable electronics by hybridizing fiber-shaped nanogenerators, solar cells, and supercapacitors. *Sci Adv* 2(10):e1600097–e1600105
6. Wang ZL (2013) Triboelectric nanogenerators as new energy technology for self-powered systems and as active mechanical and chemical sensors. *ACS Nano* 7(11):9533–9557
7. Wang ZL, Jiang T, Xu L (2017) Toward the blue energy dream by triboelectric nanogenerator networks. *Nano Energy* 39:9–23
8. Chen BD, Tang W, He C, Deng CR, Yang LJ, Zhu LP, Chen J, Shao JJ, Liu L, Wang ZL (2018) Water wave energy harvesting and self-powered liquid-surface fluctuation sensing based on bionic-jellyfish triboelectric nanogenerator.
9. *Mater Today* 21(1):88–97 Seol ML, Woo JH, Jeon SB, Kim D, Park SJ, Hur J, Choi YK (2015) Vertically stacked thin triboelectric nanogenerator for wind energy harvesting. *Nano Energy* 14:201–208
10. Phan H, Shin D-M, Jeon SH, Kang TY, Han P, Kim GH, Kim HK, Kim K, Hwang Y-H, Hong SW (2017) Aerodynamic and aeroelastic flutters driven triboelectric nanogenerators for harvesting broadband airflow energy. *Nano Energy* 33:476–484
11. Chen B, Tang W, Jiang T, Zhu L, Chen X, He C, Xu L, Guo H, Lin P, Li D (2017) Three-dimensional ultraflexible triboelectric nanogenerator made by 3D printing. *Nano Energy* 45:380–389
12. Kim D, Lee HM, Choi Y-K (2017) Large-sized sandpaper coated with solution-processed aluminum for a triboelectric nanogenerator with reliable durability. *RSC Adv* 7:137–144
13. Liu T, Liu M, Dou S, Sun J, Cong Z, Jiang C, Du C, Pu X, Hu W, Wang ZL (2018) Triboelectric-nanogenerator-based soft energy-harvesting skin enabled by toughly bonded elastomer/hydrogel hybrids. *ACS Nano* 12(3):2818–2826
14. Guo H, Li T, Cao X, Xiong J, Jie Y, Willander M, Cao X, Wang N, Wang ZL (2017) Self-sterilized flexible single-electrode triboelectric nanogenerator for energy harvesting and dynamic force sensing. *ACS Nano* 11(1):856–864
15. Yang Y, Zhou YS, Zhang H, Liu Y, Lee S, Wang ZL (2013) A single-electrode based triboelectric nanogenerator as self-powered tracking system. *Adv Mater* 25(45):6594–6601
16. Shi M, Zhang J, Han M, Song Y, Su Z, Zhang H (2016) In a single-electrode wearable triboelectric nanogenerator based on conductive & stretchable fabric. In: 2016 IEEE 29th international conference on micro electro mechanical systems (MEMS), IEEE, pp 1228–1231
17. Zhu G, Lin ZH, Jing Q, Bai P, Pan C, Yang Y, Zhou Y, Wang ZL (2013) Toward large-scale energy harvesting by a nanoparticle-enhanced triboelectric nanogenerator. *Nano Lett* 13(2):847–853

18. Wang S, Lin L, Xie Y, Jing Q, Niu S, Wang ZL (2013) Sliding-triboelectric nanogenerators based on in-plane charge-separation mechanism. *Nano Lett* 13(5):2226–2233
19. Yang Y, Zhang H, Chen J, Jing Q, Zhou YS, Wen X, Wang ZL (2013) Single-electrode-based sliding triboelectric nanogenerator for self-powered displacement vector sensor system. *ACS Nano* 7(8):7342–7351
20. Lin L, Xie Y, Niu S, Wang S, Yang PK, Wang ZL (2015) Robust triboelectric nanogenerator based on rolling electrification and electrostatic induction at an instantaneous energy conversion efficiency of $\sim 55\%$. *ACS Nano* 9(1):922–930
21. Lin L, Wang S, Niu S, Liu C, Xie Y, Wang ZL (2014) Noncontact free-rotating disk triboelectric nanogenerator as a sustainable energy harvester and self-powered mechanical sensor. *ACS Appl Mater Interfaces* 6(4):3031–3038
22. Lee S, Ko W, Oh Y, Lee J, Baek G, Lee Y, Sohn J, Cha S, Kim J, Park J (2015) Triboelectric energy harvester based on wearable textile platforms employing various surface morphologies. *Nano Energy* 12:410–418
23. Xue C, Li J, Zhang Q, Zhang Z, Hai Z, Gao L, Feng R, Tang J, Liu J, Zhang W (2014) A novel arch-shape nanogenerator based on piezoelectric and triboelectric mechanism for mechanical energy harvesting. *Nanomaterials* 5(1):36–46
24. Yang J-H, Kim Y-K, Lee JY (2015) Simplified process for manufacturing macroscale patterns to enhance voltage generation by a triboelectric generator. *Energies* 8(11):12729–12740
25. Fan F-R, Lin L, Zhu G, Wu W, Zhang R, Wang ZL (2012) Transparent triboelectric nanogenerators and self-powered pressure sensors based on micropatterned plastic films. *Nano Lett* 12(6):3109–3114
26. Li X, Tao J, Zhu J, Pan C (2017) A nanowire based triboelectric nanogenerator for harvesting water wave energy and its applications. *APL Mater* 5(7):074104–074110
27. Choi D, Yoo D, Kim DS (2015) One-step fabrication of transparent and flexible nanotopographical-triboelectric nanogenerators via thermal nanoimprinting of thermoplastic fluoropolymers. *Adv Mater* 27(45):7386–7394
28. Dahan E, Sundararajan PR (2014) Thermo-reversible gelation of rod-coil and coil-rod-coil molecules based on poly(dimethyl siloxane) and perylene imides and self-sorting of the homologous pair. *Soft Matter* 10(29):5337–5349
29. Ko YH, Nagaraju G, Yu JS (2015) Multi-stacked PDMS-based triboelectric generators with conductive textile for efficient energy harvesting. *RSC Adv* 5(9):6437–6442
30. Yang Y, Zhang H, Lin ZH, Zhou YS, Jing Q, Su Y, Yang J, Chen J, Hu C, Wang ZL (2013) Human skin based triboelectric nanogenerators for harvesting biomechanical energy and as self-powered active tactile sensor system. *ACS Nano* 7(10):9213–9222
31. Gong J, Xu B, Tao X (2017) Breath figure micromolding approach for regulating the microstructures of polymeric films for triboelectric nanogenerators. *ACS Appl Mater Interfaces* 9(5):4988–4997
32. Saurenbach F, Wollmann D, Terris B, Diaz A (1992) Force microscopy of ion-containing polymer surfaces: morphology and charge structure. *Langmuir* 8(4):1199–1203
33. Trinh VL, Chung CK (2017) A facile method and novel mechanism using microneedle-structured PDMS for triboelectric generator applications. *Small* 13:1700373–17003